

# Blood pool and tissue phase patient motion effects on $^{82}\text{Rb}$ rubidium PET myocardial blood flow quantification

Benjamin C. Lee, PhD,<sup>a</sup> Jonathan B. Moody, PhD,<sup>a</sup> Alexis Poitrasson-Rivière, PhD,<sup>a</sup> Amanda C. Melvin, MS,<sup>b</sup> Richard L. Weinberg, MD, PhD,<sup>c</sup> James R. Corbett, MD,<sup>a,b</sup> Edward P. Ficaro, PhD,<sup>a,b</sup> and Venkatesh L. Murthy, MD, PhD<sup>b</sup>

<sup>a</sup> INVIA Medical Imaging Solutions, Ann Arbor, MI

<sup>b</sup> Division of Nuclear Medicine, Department of Radiology, University of Michigan, Ann Arbor, MI

<sup>c</sup> Division of Cardiovascular Medicine, Department of Internal Medicine, University of Michigan, Ann Arbor, MI

Received Nov 22, 2017; accepted Mar 5, 2018

doi:10.1007/s12350-018-1256-1

**Background.** Patient motion can lead to misalignment of left ventricular volumes of interest and subsequently inaccurate quantification of myocardial blood flow (MBF) and flow reserve (MFR) from dynamic PET myocardial perfusion images. We aimed to identify the prevalence of patient motion in both blood and tissue phases and analyze the effects of this motion on MBF and MFR estimates.

**Methods.** We selected 225 consecutive patients that underwent dynamic stress/rest rubidium-82 chloride ( $^{82}\text{Rb}$ ) PET imaging. Dynamic image series were iteratively reconstructed with 5- to 10-second frame durations over the first 2 minutes for the blood phase and 10 to 80 seconds for the tissue phase. Motion shifts were assessed by 3 physician readers from the dynamic series and analyzed for frequency, magnitude, time, and direction of motion. The effects of this motion isolated in time, direction, and magnitude on global and regional MBF and MFR estimates were evaluated. Flow estimates derived from the motion corrected images were used as the error references.

**Results.** Mild to moderate motion (5-15 mm) was most prominent in the blood phase in 63% and 44% of the stress and rest studies, respectively. This motion was observed with frequencies of 75% in the septal and inferior directions for stress and 44% in the septal direction for rest. Images with blood phase isolated motion had mean global MBF and MFR errors of 2%-5%. Isolating blood phase motion in the inferior direction resulted in mean MBF and MFR errors of 29%-44% in the RCA territory. Flow errors due to tissue phase isolated motion were within 1%.

**Conclusions.** Patient motion was most prevalent in the blood phase and MBF and MFR errors increased most substantially with motion in the inferior direction. Motion correction focused on these motions is needed to reduce MBF and MFR errors. (J Nucl Cardiol 2019;26:1918–29.)

**Key Words:** Myocardial perfusion imaging: PET • Coronary blood flow • Coronary flow reserve • Image artifacts • Pharmacologic stress

**Electronic supplementary material** The online version of this article (<https://doi.org/10.1007/s12350-018-1256-1>) contains supplementary material, which is available to authorized users.

The authors of this article have provided a PowerPoint file, available for download at SpringerLink, which summarises the contents of the paper and is free for re-use at meetings and presentations. Search for the article DOI on SpringerLink.com.

Edward P. Ficaro and Venkatesh L. Murthy have contributed equally to this work and are co-senior authors.

Reprint requests: Benjamin C. Lee, PhD, INVIA Medical Imaging Solutions, 3025 Boardwalk St., Suite 200, Ann Arbor, MI, 8108; [blee@inviasolutions.com](mailto:blee@inviasolutions.com)

1071-3581/\$34.00

Copyright © 2018 American Society of Nuclear Cardiology.

### Abbreviations

LV	Left ventricular
MBF	Myocardial blood flow
MFR	Myocardial flow reserve
PET	Positron emission tomography
VOI	Volume of interest
TAC	Time-activity curve
LAD	Left anterior descending
LCX	Left circumflex
RCA	Right coronary artery

**See related editorial, pp. 1865–1868**

## INTRODUCTION

PET myocardial perfusion imaging has demonstrated increased accuracy for the detection of coronary artery disease (CAD) compared to other non-invasive imaging modalities. Recent data have also shown that quantification of perfusion as myocardial blood flow (MBF) and myocardial flow reserve (MFR) improves detection of CAD<sup>1,2</sup> and risk stratification for adverse cardiac outcomes.<sup>3,4</sup>

Misalignment between dynamic images due to respiratory and patient motion can induce errors in estimates of MBF and MFR. Respiratory motion is especially problematic in the left ventricle (LV) blood pool images due to the fast kinetics of the tracer and the short time sampling. Movement which results in the LV blood pool overlapping with myocardial volumes-of-interest causes an increase in those tissue time-activity curve (TAC) in the blood pool images and a decrease in all tissue TACs in the later tissue images. Consequently, the spillover constant is overestimated and the K1 uptake parameter is also overestimated, leading to artifactually elevated MBF estimates. The LV blood pool TACs can also decrease due to movement of the LV blood pool away from the LV blood pool volume-of-interest. The result is a significant increase in MBF estimates. If these misalignments do not happen equally during both stress and rest, the MFR values are also affected.

Prior studies have measured motion from higher spatial and temporal resolution MR or CT images from hybrid PET/MR and PET/CT systems<sup>5–7</sup> and other studies have measured respiratory motion using tracking markers or sensors.<sup>7–10</sup> Data-driven approaches which only utilize the reconstructed images have the advantages of being fast, inexpensive, and robust.<sup>11–15</sup> Yet these data-driven motion analysis studies have only focused on the later tissue-phase frames (> 90 seconds after injection).<sup>12–14</sup> A recent study found patient motion shifts of up to 20 mm result in MBF errors of up to 500% in simulations but confirmation with clinical data and clinically observed shifts is needed.<sup>13</sup>

The purpose of the study is (a) to identify the prevalence of patient motion in dynamic rubidium-82 chloride (<sup>82</sup>Rb) PET myocardial perfusion images across the entire dynamic sequence, (b) to investigate the effects of this motion on MBF and MFR estimates, and (c) to provide guidance as to how motion can be properly corrected.

## MATERIALS AND METHODS

### Study Population

We evaluated dynamic <sup>82</sup>Rb rest and stress images from 225 sequentially selected patients that were referred for clinically indicated <sup>82</sup>Rb rest and stress imaging between June 1, 2017 and July 26, 2017. All subjects provided written informed consent and all exam protocols were approved by the University of Michigan Institutional Review Board.

### PET Imaging

All subjects were instructed to avoid caffeine and methylxanthine intake for 24 hours and to fast overnight prior to PET imaging. <sup>82</sup>Rb was administered using a weight-adjusted protocol of 12 MBq/kg (0.32 mCi/kg) using the same activity (481–1665 MBq [13–45 mCi]) for both rest and stress. <sup>82</sup>Rb was directly eluted from a generator and infused into a brachial vein at 50 mL/min over 5–25 seconds using the Cardiogen-82 infusion system (Bracco Diagnostics, Monroe Township, NJ). Dynamic PET scans were acquired in 3D list mode over 6 minutes and 40 seconds from the point of radiotracer injection on a Biograph mCT whole-body PET/CT scanner (Siemens Healthcare USA, Malvern, PA). Pharmacological stress was performed using a bolus injection of 0.4 mg of intravenous regadenoson over 15 seconds followed by a 10-mL flush. Then 45 seconds after the regadenoson injection, the stress <sup>82</sup>Rb infusion was administered and the second dynamic PET scan was acquired with the same scan length.

### Image Processing

Dynamic <sup>82</sup>Rb emission images were reconstructed using attenuation-weighted iterative 3D ordered-subset expectation-maximization iterative reconstruction or 3D-OSEM with 21 subsets and 3 iterations with point-spread-function (PSF) and time-of-flight (TOF) modeling, standard corrections including randoms, attenuation, scatter, and prompt gamma, and without post-filtering. Images were reconstructed to a matrix size of 128 × 128 and pixel size of 3.18 × 3.18 mm. A 30-frame dynamic reconstruction was performed over 6 minutes and 40 seconds<sup>16</sup> with 5-second initial blood-phase frame durations<sup>17</sup>: 16 × 5, 6 × 10, 3 × 20, 4 × 30, 1 × 80 seconds.

Minimal 3D spatial smoothing was applied to the image volume using a 1-12-1 weighted averaging filter in three dimensions. LV myocardial surfaces were automatically determined using the Corridor4DM software (INVIA, Ann

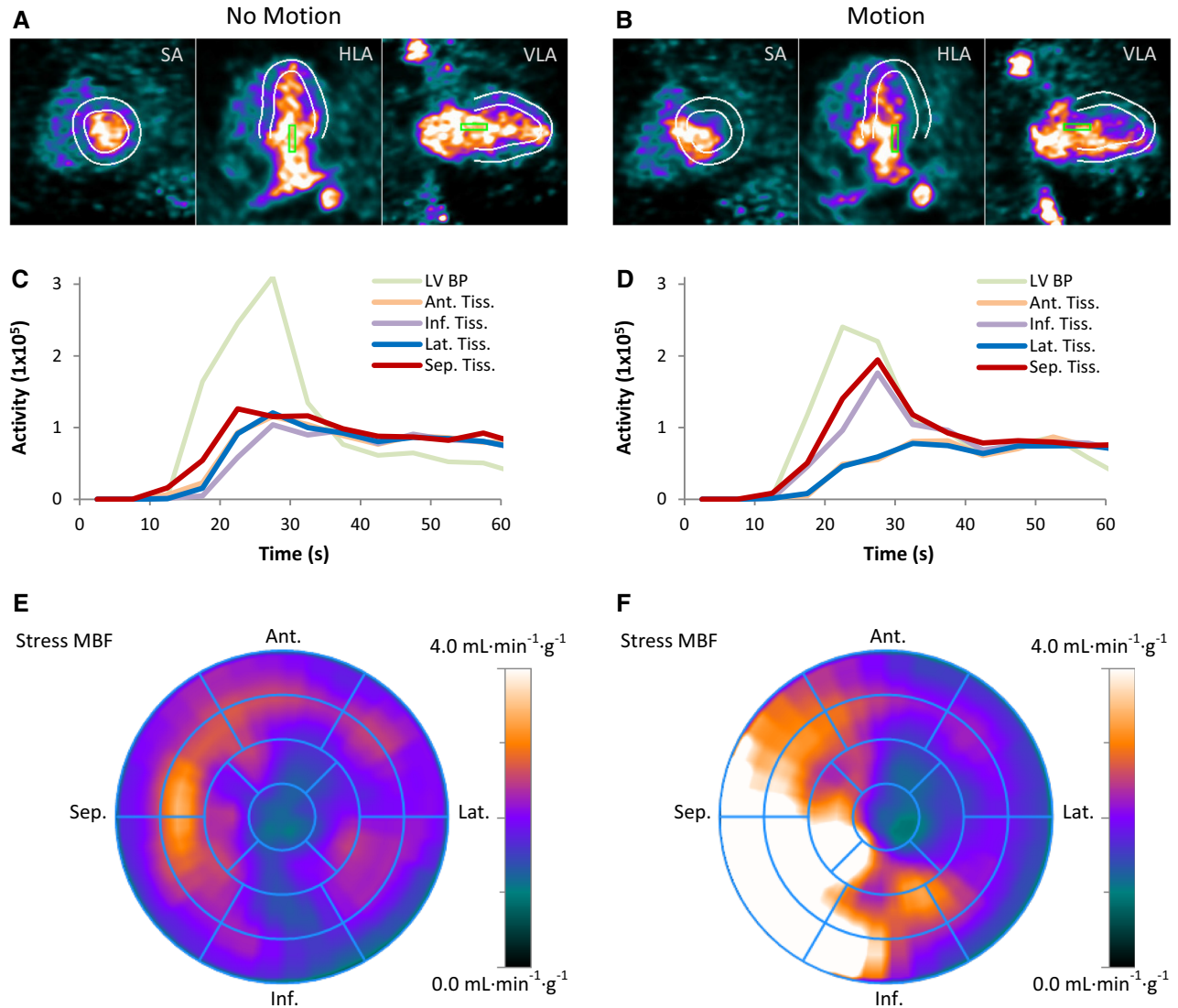


**Figure 1.** Shift example of a stress study (Patient 110) at the 25- to 30-second frame in cardiac views (A) with no motion and (B) with motion of 12.8, 10.2, and 6.8 mm in the septal, inferior, and apical directions, respectively, where the green box is the LV blood pool (LV BP) volume-of-interest. Regional TACs (C) with no motion and (D) with motion, where blood pool spillover in the myocardium is less uniform. MBF polar map value increases to the greatest in the basal inferoseptal segment outside of the expected clinical range from (E)  $2.0 \text{ mL}\cdot\text{min}^{-1}\cdot\text{g}^{-1}$  with no motion to (F)  $7.9 \text{ mL}\cdot\text{min}^{-1}\cdot\text{g}^{-1}$  with motion. Global MBF increases by 15% from  $2.0 \text{ mL}\cdot\text{min}^{-1}\cdot\text{g}^{-1}$  with no motion to  $2.3 \text{ mL}\cdot\text{min}^{-1}\cdot\text{g}^{-1}$  with motion.

Arbor, MI) that utilized a myocardial volume summed from the data acquired from 2 to 6 minutes and 40 seconds.<sup>18</sup>

### Manual Motion Correction

Motion correction was manually performed on each set of dynamic frames by one of three physician readers. LV myocardial surfaces generated from the summed static uptake images were used as the motion references. For each temporal frame in each dataset, the reader shifted short-axis, horizontal

long-axis, and vertical long-axis images in each of the 3-coordinate axes ( $x$ ,  $y$ ,  $z$ ) as shown in Figure 1A, B. In this study, the temporal sampling protocol was divided into two phases: (1) a finely sampled (5- to 10-second frame durations) dynamic blood phase from 0 to 120 seconds that encompassed the blood pool input function, and (2) a coarsely sampled (e.g., 30 seconds) slow-varying tissue phase that spanned from 2 minutes to the end of the acquisition.

In the blood phase, the criteria for coregistration were: (a) LV blood pool activity centered within the LV endocardial

**Table 1.** Subject characteristics

Characteristic	Patients (n = 225)
Age (year)	65 [57–72]
Weight (kg)	95 [75–116]
Height (m)	1.7 [1.6–1.8]
BMI (kg·m <sup>-2</sup> )	32 [27–40]
BMI ≥ 30 kg·m <sup>-2</sup>	138 (61)
Male	130 (58)
Hypertension	183 (81)
Dyslipidemia	159 (71)
Diabetes	103 (46)
Any prior CAD	71 (32)
Stress LVEF (%)	65 [55–72]
Rest LVEF (%)	62 [53–68]
Summed stress score	0.0 [0.0–8.0]
Summed rest score	0.0 [0.0–3.0]
Summed difference score	0.0 [0.0–3.0]
Global MFR	2.0 [1.5–2.4]
Stress global MBF (mL·min <sup>-1</sup> ·g <sup>-1</sup> )	2.1 [1.6–2.7]
Rest global MBF (mL·min <sup>-1</sup> ·g <sup>-1</sup> )	1.1 [0.8–1.3]

MFR and MBF values are motion corrected. Continuous variables are presented as median [interquartile range]. Dichotomous variables are presented as number (%). BMI, indicates body mass index; CAD, coronary artery disease; LVEF, left ventricular ejection fraction; MFR, myocardial flow reserve; MBF, myocardial blood flow

surface, (b) no overlap between the left atrial blood pool and the septal myocardial wall and (c) uniform blood pool spillover in the LV myocardial surfaces except for the apex where greater spillover was expected due to a thinner myocardial wall and greater cardiac wall thickening as shown in Figure 1A. In the transition frames of the blood phase where the activity has cleared the LV blood pool and a distinction between the blood pool and tissue activities was difficult to observe, the objective was to center the LV activity within the LV epicardial surface.

In the tissue phase, the criterion for coregistration was to center LV tissue activity within the LV myocardial surfaces. These shifts were recorded as three-dimensional translational motion vectors for each frame. The generated LV myocardial surfaces assumed a uniform thickness resulting in biases in the shifts in the thinner apical region. All shifts were recomputed relative to the final summed image.

Inter-reader mean differences in motion correction shifts between the 3 readers were tested for insignificance so that all studies could be combined into a single population. A linear mixed-effects model with per subject error terms to account for correlation between the stress and rest data from a given series was used for the 3 directional motion shifts across all 30 frames, 2 series, and 3 readers as fixed effects. Since there

were statistically insignificant mean differences between the 3 readers for all three directions (basal–apical [ $P = .894$ ], septal–lateral [ $P = .518$ ], and inferior–anterior [ $P = .785$ ]), the motion correction shifts from each reader were used as the reference motion vectors for this study.

### Motion Analysis on Frequency, Magnitude, Time, and Direction

The motion shift magnitudes for the blood and tissue phases were calculated across all patients at stress and rest. These were categorized as “none” for 0 mm shifts, “minimal” for over 0–5 mm shifts, “mild” for 5–10 mm shifts, “moderate” for 10–15 mm shifts, “severe” for 15 mm or greater shifts. The magnitude of the motion shift from the frame with the peak LV blood pool activity was used for the blood phase because it has the greatest influence on the area-under-the-curve of the dynamic LV input function. However, the maximum magnitude of the motion shift in the tissue frames was used for the tissue phase to observe deviations from the static reference image. Motion direction for each frame was calculated across all patients with minimal or larger motion shifts, along the three axes (basal–apical, septal–lateral, and inferior–anterior) at stress and rest.

### Blood Pool and Tissue Sampling

The volume-of-interest (VOI) sampling methodology used a 3D rectangular VOI that was centered at the mitral valve plane in parallel to the long-axis of the LV to automatically extract a unique LV blood pool time-activity curve. The size of the box was 2 × 2 pixels wide (6.4 mm) to minimize spillover from the myocardium and spanned in the direction of the long-axis to include activity in both the LV and left atrium (6.4 × 6.4 × 30 mm). The myocardial tissue time-activity curves were estimated from the tracer activity midway between the endocardial and epicardial surfaces for each of the 17-segment regions, the 3 vascular territories of the left anterior descending (LAD), left circumflex (LCX), and right coronary artery (RCA), and the whole left ventricle (global). Blood pool and tissue activities were sampled both with no motion as shown in Figure 1C and with motion as shown in Figure 1D for comparison of blood flow estimation in Figure 1E, F, respectively.

### Blood Flow Estimation

Both the LV blood pool input function and LV tissue TACs were fit to a 1-tissue compartment model to obtain estimates for uptake rate  $K_1$ , washout rate  $k_2$ , and LV blood pool to myocardium spillover  $f_v$ . Myocardial blood flow was computed from the estimated  $K_1$  using a previously validated  $K_1$ -MBF relationship for <sup>82</sup>Rb.<sup>19</sup> All temporal frames were frame duration weighted in the kinetic fitting. Global and vascular territory MBF and MFR values were computed with no motion correction and with motion correction.

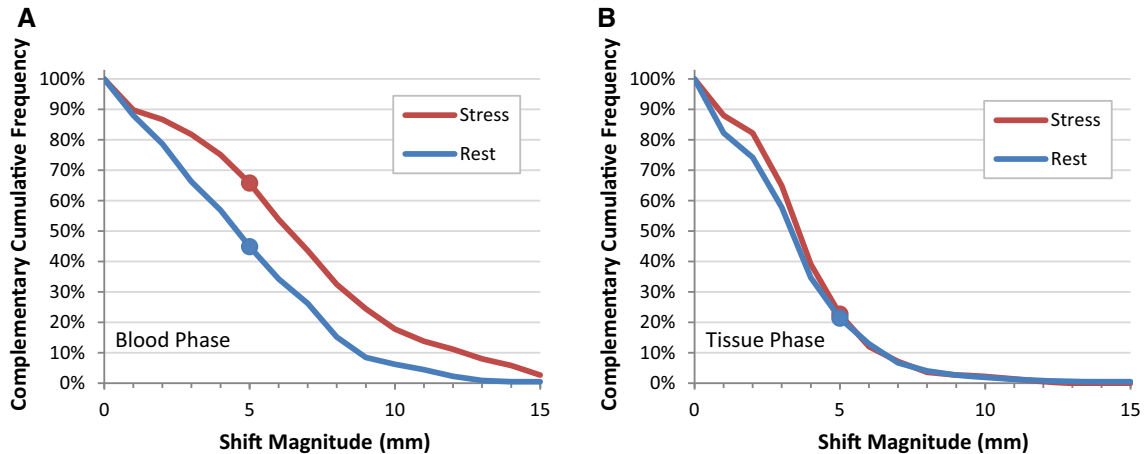


**Figure 2.** Complementary cumulative frequency distributions show percentage of PET datasets with shift magnitudes greater than or equal to a particular value for the (A) blood phase and (B) tissue phase. The shift magnitude at the peak LV frame is used for the blood phase and the maximum shift magnitude is used in the tissue phase. Circles indicate the percent of shift magnitudes  $\geq 5$  mm (mild, moderate, and severe) that in the blood phase are 66% and 45% for stress and rest datasets, and in the tissue phase are 23% and 21% for stress and rest datasets, respectively.

### Temporally and Spatially Isolated Motion Effects on MBF and MFR

Relative changes in global and regional MBF or MFR by isolating phase (temporal) and direction (spatial) were computed. The MBF and MFR values from the motion corrected dynamic sequences were the reference values for computing relative changes and were defined as “errors” within this study to eliminate the ambiguity of whether the motion uncorrected or motion corrected images are the reference. Blood-phase isolation was achieved by only applying motion correction in the tissue phase so that the flow errors were a result of motion in the blood phase, and vice versa for the tissue-phase isolation. Isolated directional motion was achieved by applying motion corrections in all directions except for the isolated direction of interest. Combination of temporal and spatial motion isolations further narrowed the source of the motion. For example, to isolate the effect of motion in the inferior–anterior direction during the blood phase, only motion correction in the basal–apical and septal–lateral were applied in the blood phase but motion correction in all directions was applied in the tissue phase. The impact of motion severity on flow errors was selectively assessed based on motion magnitude categories previously defined. Smoothed 17-segmental flow error polar maps and vascular flow errors were computed to observe the greater regional impact of the motion compared to the average effect on the global flow.

### Statistical Analysis

Statistical significance was assessed with Wilcoxon rank sum tests and Kruskal–Wallis rank sum tests for independent variables with two and three levels, respectively, and a one-sample *t* test. Two-sided values of  $P < .05$  were considered

significant. All statistical analyses were performed with R 3.3.1 (The R Foundation for Statistical Computing).

## RESULTS

### Study Population

Characteristics of patients evaluated are given in Table 1. The cohort consisted of 130 men and 95 women, age  $64 \pm 12$  years with a high prevalence of coronary risk factors.

### Motion Magnitude and Frequency

In the blood phase, the greatest frequencies of peak LV blood pool motion shifts were mild (48%) then minimal (27%) for stress datasets but a reverse order of minimal (45%) then mild (39%) for rest datasets (Supplemental Table 1). Therefore, mild to severe shift magnitudes ( $\geq 5$  mm) were present in 66% of the stress datasets and 45% of the rest datasets (Figure 2A). The median shift in any direction during the blood phase was 6.4 mm for stress datasets and 4.5 mm for rest datasets.

In the tissue phase, the greatest frequencies of maximum magnitude of the motion shifts in the tissue phase were minimal (66%) then mild (20%) for stress datasets and similarly minimal (64%) then mild (20%) for rest datasets (Supplemental Table 1). Therefore, mild to severe shift magnitudes ( $\geq 5$  mm) were present in 23% of the stress datasets and 21% of the rest datasets (Figure 2B). The median shift in any direction during



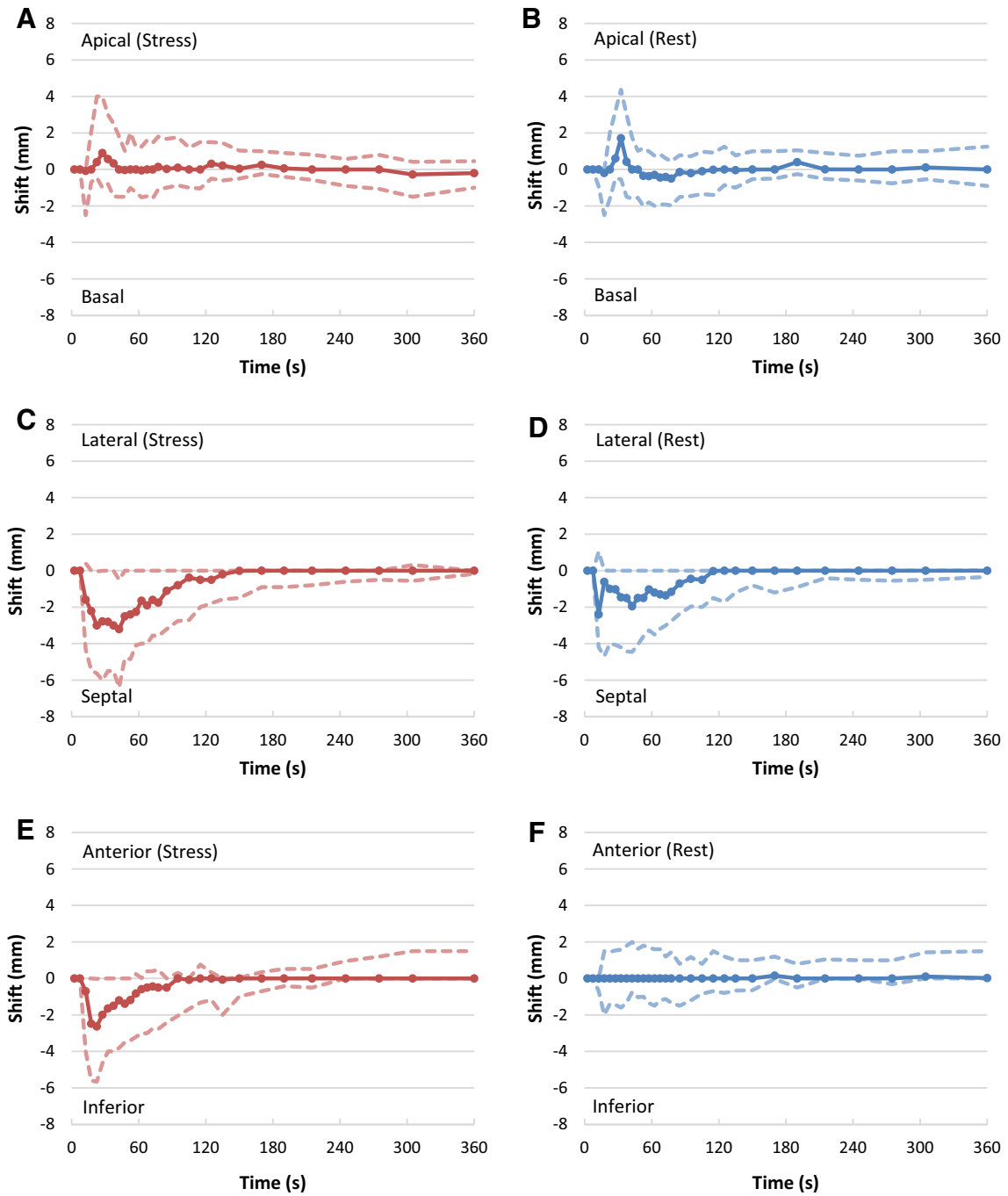


**Figure 3.** Median motion shifts per time across stress datasets in the (A) basal–apical, (C) septal–lateral, and (E) inferior–anterior directions, and across rest datasets in the (B) basal–apical, (D) septal–lateral, and (F) inferior–anterior directions. Solid line indicates median and dashed lines indicate the 25th and 75th percentiles.

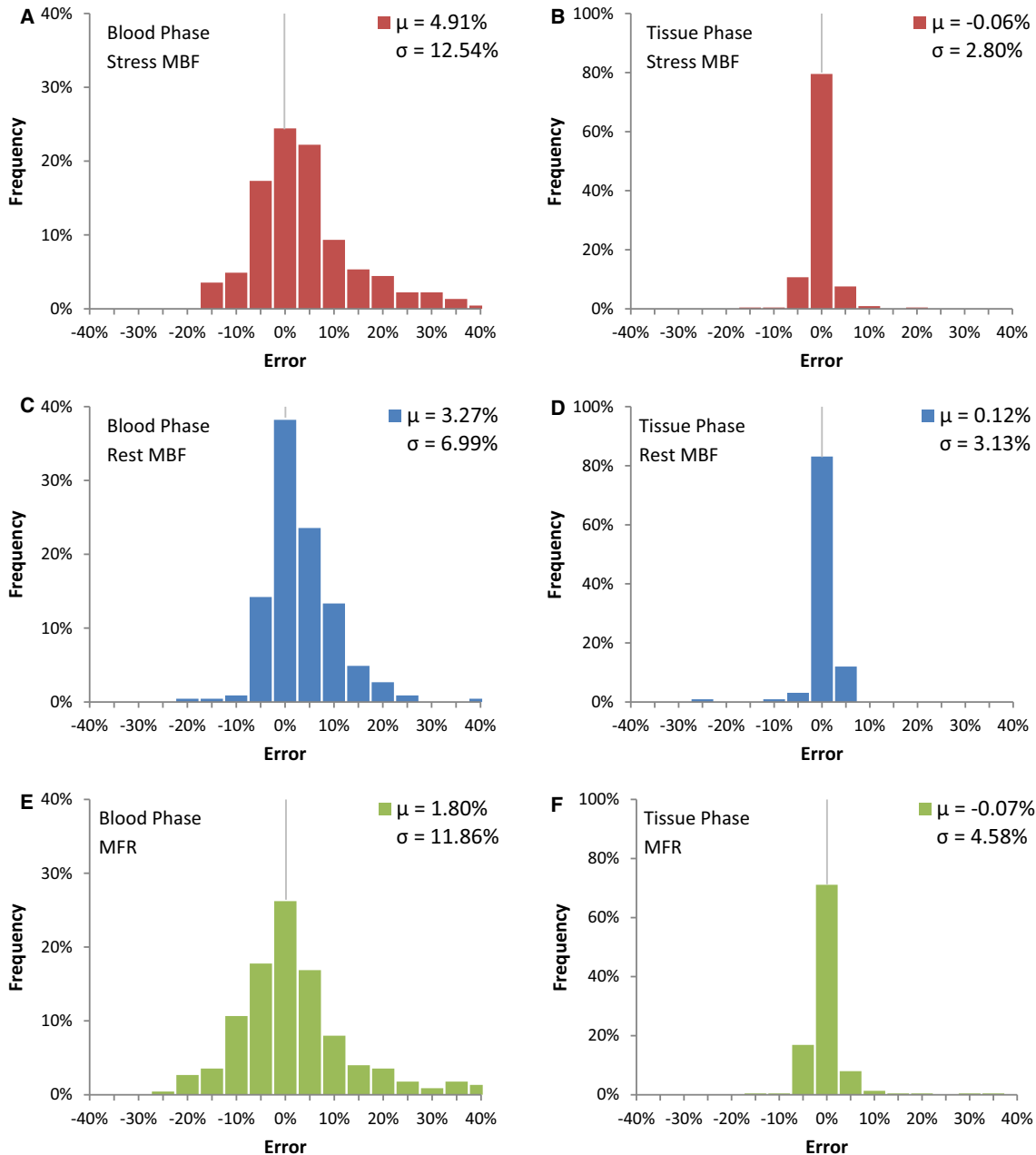


**Figure 4.** Blood-phase isolated motion effects on global (A) stress MBF, (C) rest MBF and (E) MFR, and tissue-phase isolated motion effects on global (B) stress MBF, (D) rest MBF and (F) MFR, across all datasets.  $\mu$  is the mean error and  $\sigma$  is the standard deviation of the error.

the tissue phase was 3.5 mm for stress datasets and 3.3 mm for rest datasets.

### Motion Direction and Time

The median blood-phase motion shifts with the peak LV blood pool activity exceeded 2 mm in both the septal and inferior directions for stress (Figure 3C, E) but only in the septal direction for rest (Figure 3D). The

blood-phase motion shifts were significant in all directions for stress and rest ( $P < .0001$ ) (Figure 3A-E) except for the inferior direction at rest ( $P = .27$ ) (Figure 3F). They were greatest in the septal direction with a mean shift of 3.4 mm, followed by the inferior direction with a mean shift of 2.9 mm, and the least in the apical direction with a mean shift of 2.1 mm for stress datasets. The blood-phase motion mean shifts for rest datasets were 2.2 mm in the septal direction and

1.3 mm in the apical direction (Supplemental Table 3). Though the blood-phase shifts were not equally distributed in all directions. The most frequent directions of mild to moderate motion magnitudes were septal (28%) then inferior (20%) for stress datasets, followed by septal (20%) then apical (12%) for rests datasets (Supplemental Table 2). The blood phase shifts were also not equally distributed in time. Mean time of peak LV blood pool activity with mild to moderate motion was  $27 \pm 7$  seconds for stress and rest.

The middle 50% of the maximum-magnitude tissue-phase motion shifts were less than 2 mm in magnitude (Figure 3). Though, the tissue-phase motion shifts were significant in all directions at stress ( $P \leq .0040$ ) but only in the septal direction at rest ( $P < .0001$ ) (Figure 3D). They were greatest in the septal direction with a mean shift 1.1 mm, followed by the inferior direction with a mean shift of 0.6 mm, and the least in the apical direction with a mean shift of 0.5 mm for stress datasets. The tissue-phase motion mean shift for rest datasets in the septal direction was 0.9 mm (Supplemental Table 3).

The blood-phase motion shifts were significantly different between stress and rest datasets in the septal ( $P = .0006$ ) and inferior ( $P < .0001$ ) directions, but not in the apical direction ( $P = .061$ ). Stress and rest datasets for the tissue-phase motion shifts were only significantly different in the inferior direction ( $P = .0004$ ) but not in the apical ( $P = .25$ ) or septal ( $P = .23$ ) directions.

### Isolated Phase Motion Effects on MBF and MFR

In Figure 4, all motion in the blood phase introduced mean errors of  $4.9\% \pm 12.5\%$  in stress MBF,  $3.3\% \pm 7.0\%$  in rest MBF, and  $1.8\% \pm 11.9\%$  in MFR. Motion in the tissue phase introduced mean errors of  $-0.1\% \pm 2.8\%$  in stress MBF,  $0.1\% \pm 3.1\%$  in rest MBF, and  $-0.1\% \pm 4.6\%$  in MFR. For all error comparisons, the larger magnitude blood-phase motions introduced errors with greater bias and variance than those of tissue-phase motions.

### Isolated Directional Motion Effects on MBF and MFR

The influence of the mild to moderate blood-phase motion shifts on regional stress MBF, rest MBF and MFR errors (per column) are shown for the all, apical, septal, and inferior directions (per row) in polar map format in Figure 5. Motion in all directions induced a maximum error of 36% in the stress MBF and 26% in rest MBF in the basal inferoseptal segment (Figure 5A, B) with a corresponding error of 23% in MFR (Figure 5C). Motion in the apical direction induced a

maximum error of 29% in stress MBF and 42% in the rest MBF in the apex segment (Figure 5D, E) yet the MFR error in the same segment was only 2% due to canceling of errors in the MFR ratio of stress MBF to rest MBF (Figure 5F). Motion in the septal direction induced a maximum error of 33% in the stress MBF and 24% in the rest MBF in again in the basal inferoseptal segment (Figure 5G, H), leading to an error of 11% in MFR in the same segment (Figure 5I). The largest effect on flow was caused by motion in the inferior direction resulting in a maximum error of 69% in the stress MBF and 37% in rest MBF in the basal inferior segment with a corresponding error of 54% in MFR (Figure 5L).

When including datasets with all motions from none to severe, linear relationships were observed between MBF errors and blood phase motion shifts. The expected MBF error per 5-mm shift is 6% for stress LAD with apical motion ( $R = 0.46$ ), 8% for stress LCX with septal motion ( $R = 0.62$ ), and 27% for stress RCA with inferior motion ( $R = 0.76$ ). Scatter plots with linear regressions of regional stress MBF errors in each isolated direction are presented in detail in Supplemental Figure 1.

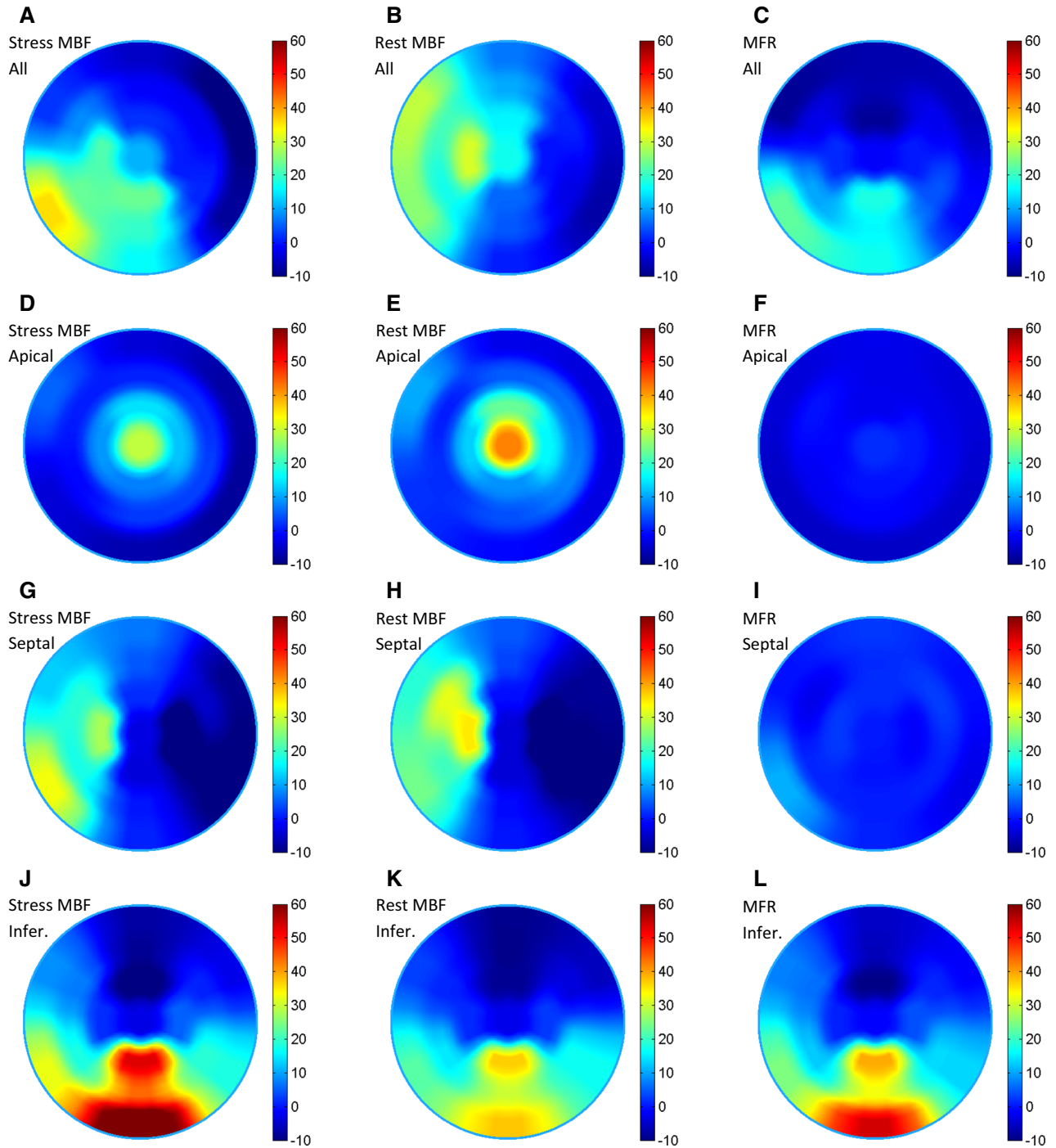
Minimal motion shifts in the blood phase introduced global flow errors of 2%-5%, while minimal motion shifts during the tissue phase introduced global flow errors of 1%, in part due to smaller shifts (Figure 2, Supplemental Table 3). Mild-moderate inferior-isolated motion in the blood-phase induced the greatest flow errors in the RCA territory with a 44% error in stress MBF, 29% error in rest MBF, and 34% error in MFR when averaged over all datasets. The global and regional stress MBF, rest MBF and MFR mean errors per time phase, motion shift magnitude, and isolated direction are presented in detail in Supplemental Table 4.

Table 2 shows the comparison of flow results with and without manual motion correction globally and for each vascular territory. MBF and MFR values with motion were significantly higher in all cases except for global MFR and MFR in the LCX territory.

## DISCUSSION

This study quantitatively confirmed that motion was common with greater magnitude in the blood phase, where 55% of datasets had motion  $\geq 5$  mm, than in the tissue phase, particularly in the septal and inferior directions. We also showed that there was significantly more motion in stress than in rest datasets. When applying these observed motion characteristics in isolation to the real data, blood phase motion often had meaningful clinical effects, where 45% of datasets had MBF errors  $> 5\%$  in magnitude.





**Figure 5.** Mean relative flow percent error polar maps vs. mild-moderate (5-15 mm) direction-isolated motion across all datasets. Flows with expert motion corrections are the references. Rows vary the direction of blood-phase isolated motion in (A, B, C) all, (D, E, F) apical, (G, H, I) septal, and (J, K, L) inferior directions. Columns vary the effect on the flow for (A, D, G, J) stress MBF, (B, E, H, K) rest MBF, and (C, F, I, L) MFR.

**Table 2.** Flow results

Quantity	Region	No motion	Motion	<i>P</i>
Stress MBF	Global	2.21 ± 0.89	2.32 ± 1.00	< .0001
	LAD	2.29 ± 0.91	2.36 ± 0.98	.0013
	LCX	2.09 ± 0.91	2.05 ± 0.91	.018
	RCA	2.10 ± 0.99	2.59 ± 1.45	< .0001
Rest MBF	Global	1.11 ± 0.40	1.15 ± 0.40	< .0001
	LAD	1.16 ± 0.41	1.23 ± 0.44	< .0001
	LCX	1.10 ± 0.42	1.08 ± 0.39	.0007
	RCA	1.00 ± 0.38	1.06 ± 0.44	< .0001
MFR	Global	2.05 ± 0.69	2.09 ± 0.73	.084
	LAD	2.06 ± 0.68	1.99 ± 0.67	.0004
	LCX	1.97 ± 0.69	1.96 ± 0.66	.67
	RCA	2.17 ± 0.85	2.55 ± 1.33	< .0001

*MBF*, myocardial blood flow is in mL·min<sup>-1</sup>·g<sup>-1</sup>, and *MFR*, myocardial flow reserve is unitless. Flows are presented as mean ± standard deviation. *P* values compare No motion and Motion flows

While prior motion analysis studies have focused on the later tissue-phase frames where periodic respiratory motion is averaged out in the longer duration frames, they have not evaluated motion in the early blood pool frames,<sup>12–14</sup> or they have only observed effects on flow estimates through simulations using digital phantoms.<sup>13</sup> Other data-driven studies were qualitative using a categorical scoring system (e.g., 0–3) for severity of motion and did not provide quantitative results.<sup>12,13</sup> One study did develop a motion analysis algorithm across the whole dynamic sequence but did not establish a truth as a baseline for comparison which was more problematic since they were not able to confidently measure motion of the blood pool along the long-axis.<sup>15</sup>

### Motion Prevalence

Moderate to severe motion was more prevalent in the blood phase than in the tissue phase (with summed tissue image as reference), possibly due to shorter frame durations and respiratory motion, fast kinetics, and patient discomfort (Figures 2 and 3). Furthermore, greater motion was observed at stress than at rest (Figures 2 and 3). This was especially the case in the inferior direction where the significant difference in mean displacement was 2.7 mm reflecting upward creep of the heart, possibly due to deep respiration at the start of stress (Figure 3 and Supplemental Table 3).<sup>20</sup> The impact of the stress agent on motion was reported in a prior study with regadenoson resulting in substantially lower motion compared with adenosine.<sup>14</sup> This study exclusively used regadenoson and thus greater motion is possible with another stress agent.

### Effects on Flow Estimates

Large errors in stress MBF, rest MBF, and MFR (> 5%) attributable to blood-phase motions were extremely common, occurring in 54%, 36%, and 52% of the datasets, respectively. Impact of motion during the tissue phase was more limited with errors > 5% in stress MBF, rest MBF, and MFR in only 6%, 4%, and 11% of the datasets, respectively (Figure 4). Prior work with simulations showed the effect on MBF error to be significantly higher in the 1- to 2-minute range compared to close to the start or at the end of the scan.<sup>13</sup>

The greater the magnitude of motion, the greater the impact on biasing the flow estimates. Generally, there was a relationship between an increase in motion in one direction and an increase in MBF error in the myocardial region located in the same direction. This was most obvious for mild-moderate motion in the inferior direction resulting in up to an average 55% stress MBF error in the inferior region and average 44% stress MBF error in the overlapping RCA territory. If one is only concerned with MFR estimates, then mild-moderate shifts in the apical and septal directions result in less than 10% magnitude MFR error because of the similar errors both their stress MBF and rest MBF canceling out (Figure 5). Motion in all directions resulted in lower average errors because the effects were distributed over a wider range than concentrating in one direction (Figure 5, Supplemental Table 4).

While it was shown that motion artefacts at higher spatial resolutions lead to great MBF errors, greater reduction in MBF error was accomplished by motion correction (96% error reduction) rather than post-smoothing (65% error reduction).<sup>13</sup> Additionally,

minimal post-reconstruction smoothing is the recommendation for MBF quantification as excessive filtering increases spillover from extracardiac activity and bias in MBF estimates.<sup>21</sup>

### Motion Correction Recommendations

Recommendations for motion correction to minimize MBF and MFR errors are to prioritize correcting motion in the frames with the greatest blood pool. Focus should be paid to inferior motion, particularly for stress datasets. Then the blood phase motion in the septal direction for stress should be addressed next followed by blood phase motion in the septal direction for rest. Correcting motion in the tissue phase is more susceptible to user variability due to lower count statistics and had the least impact on flow estimates with reduction in error of less than 1% (Supplemental Table 4). Consequently, focus should be on correcting only large amplitude motion during the tissue phase. Additionally, care should be paid to quality control tissue volume-of-interest identification, with attention to the apex. Motion in the apical direction should be corrected sparingly for severe motion only.

Critically, for scenarios where these types of motion are not corrected, biases in all global and regional stress and rest MBF estimates and in just LAD and RCA regional MFR estimates can be expected (Table 2).

### Limitations

This study lacked an absolute truth for the motion vectors as physician reader motion vectors were used as the reference. Inter-user variability testing of the motion shifts between the 3 readers was not performed on the study population. Tissue phase summed images affected by interframe motion will be blurrier and may be an inaccurate motion reference image. Intra-frame motion including cardiac motion and respiratory motion in the longer duration frames were not studied. Rotational and non-rigid motions were also not corrected.

Only post-reconstruction corrections were made by the readers not accounting for any CT-based attention correction (CTAC) misalignment effects. Misalignments between PET and CT for attenuation correction during the dynamic sequence require varying registrations, which were not performed in this study because it was not available on the system. Variations in other methodological factors such as scatter correction, prompt gamma correction, temporal sampling, image reconstruction and post-filtering, and tracer kinetic modeling could also affect the results.

This study only used regadenoson and other stress agents, such as adenosine or dipyridamole, may result in different motion displacements.

### NEW KNOWLEDGE GAINED

Patient motion between 5 and 15 mm in the inferior direction in the early blood phase frames of stress dynamic <sup>82</sup>Rb PET datasets occurs in 20% of all cases and on average increases MBF and MFR error up to 10% globally and up to 44% in the RCA territory.

### CONCLUSIONS

Patient motion during dynamic perfusion PET is common and can cause meaningful errors in MBF and MFR estimates, particularly in the RCA territory. Motion correction is necessary to reduce bias in MBF and MFR.

### Disclosures

*B.C. Lee, J.B. Moody, and A. Poitrasson-Rivière are employees of INVIA Medical Imaging Solutions. A.C. Melvin and R.L. Weinberg have no disclosures. J.R. Corbett and E.P. Ficaró are owners of INVIA Medical Imaging Solutions. V.L. Murthy has received consulting fees from Ionetix, Inc, and owns stock in General Electric and Cardinal Health and stock options in Ionetix, Inc. V.L. Murthy is supported by 1R01HL136685 from the National, Heart, Lung, Blood Institute, and research grants from INVIA Medical Imaging Solutions and Siemens Medical Imaging.*

### References

1. Naya M, Murthy VL, Taqueti VR, Foster CR, Klein J, Garber M, et al. Preserved coronary flow reserve effectively excludes high-risk coronary artery disease on angiography. *J Nucl Med* 2014;55:248–55. <https://doi.org/10.2967/jnumed.113.121442>.
2. Ziadi MC, deKemp RA, Williams K, Guo A, Renaud JM, Chow BJW, et al. Does quantification of myocardial flow reserve using rubidium-82 positron emission tomography facilitate detection of multivessel coronary artery disease? *J Nucl Cardiol* 2012;19:670–80. <https://doi.org/10.1007/s12350-011-9506-5>.
3. Murthy VL, Naya M, Foster CR, Hainer J, Gaber M, Di Carli G, et al. Improved cardiac risk assessment with noninvasive measures of coronary flow reserve. *Circulation* 2011;124:2215–24. <https://doi.org/10.1161/CIRCULATIONAHA.111.050427>.
4. Ziadi MC, deKemp RA, Williams KA, Guo A, Chow BJW, Renaud JM, et al. Impaired myocardial flow reserve on rubidium-82 positron emission tomography imaging predicts adverse outcomes in patients assessed for myocardial ischemia. *J Am Coll Cardiol* 2011;58:740–8. <https://doi.org/10.1016/j.jacc.2011.01.065>.
5. Chun SY, Reese TG, Ouyang J, Guerin B, Catana C, Zhu X, et al. MRI-based nonrigid motion correction in simultaneous PET/MRI. *J Nucl Med* 2012;53:1284–91. <https://doi.org/10.2967/jnumed.111.092353>.

6. Küstner T, Schwartz M, Martirosian P, Gatidis S, Seith F, Gilliam C, et al. MR-based respiratory and cardiac motion correction for PET imaging. *Med Image Anal* 2017;42:129–44. <https://doi.org/10.1016/j.media.2017.08.002>.
7. Lamare F, Le Maitre A, Dawood M, Schäfers KP, Fernandez P, Rimoldi OE, et al. Evaluation of respiratory and cardiac motion correction schemes in dual gated PET/CT cardiac imaging: Motion correction strategies in dual gated cardiac. *Med Phys* 2014;41:072504. <https://doi.org/10.1118/1.4881099>.
8. Naum A, Laaksonen MS, Tuunanen H, Oikonen V, Teräs M, Kemppainen J, et al. Motion detection and correction for dynamic 15O-water myocardial perfusion PET studies. *Eur J Nucl Med Mol Imaging* 2005;32:1378–83. <https://doi.org/10.1007/s00259-005-1846-4>.
9. Koshino K, Watabe H, Enmi J, Hirano Y, Zeniya T, Hasegawa S, et al. Effects of patient movement on measurements of myocardial blood flow and viability in resting 15O-water PET studies. *J Nucl Cardiol* 2012;19:524–33. <https://doi.org/10.1007/s12350-012-9522-0>.
10. Yu Y, Chan C, Ma T, Liu Y, Gallezot J-D, Naganawa M, et al. Event-by-event continuous respiratory motion correction for dynamic PET imaging. *J Nucl Med* 2016;57:1084–90. <https://doi.org/10.2967/jnumed.115.167676>.
11. Kesner AL, Schleyer PJ, Büther F, Walter MA, Schäfers KP, Koo PJ. On transcending the impasse of respiratory motion correction applications in routine clinical imaging: A consideration of a fully automated data driven motion control framework. *EJNMMI Phys* 2014;1:8. <https://doi.org/10.1186/2197-7364-1-8>.
12. Woo J, Tamarappoo B, Dey D, Nakazato R, Le Meunier L, Ramesh A, et al. Automatic 3D registration of dynamic stress and rest <sup>82</sup>Rb and flurpiridaz F 18 myocardial perfusion PET data for patient motion detection and correction: Automated PET motion correction. *Med Phys* 2011;38:6313–26. <https://doi.org/10.1118/1.3656951>.
13. Hunter CRRN, Klein R, Beanlands RS, deKemp RA. Patient motion effects on the quantification of regional myocardial blood flow with dynamic PET imaging: Patient motion effects on regional myocardial blood flow. *Med Phys* 2016;43:1829–40. <https://doi.org/10.1118/1.4943565>.
14. Memmott MJ, Tonge CM, Saint KJ, Arumugam P. Impact of pharmacological stress agent on patient motion during rubidium-82 myocardial perfusion PET/CT. *J Nucl Cardiol* 2017. <https://doi.org/10.1007/s12350-016-0767-x>.
15. Turkington TG, DeGrado TR, Hanson MW, Coleman RE. Alignment of dynamic cardiac PET images for correction of motion. *IEEE Trans Nucl Sci* 1997;44:235–42. <https://doi.org/10.1109/23.568814>.
16. Efseaff M, Klein R, Ziadi MC, Beanlands RS, deKemp RA. Short-term repeatability of resting myocardial blood flow measurements using rubidium-82 PET imaging. *J Nucl Cardiol* 2012;19:997–1006.
17. Lee BC, Moody JB, Weinberg RL, Corbett JR, Ficaro EP, Murthy VL. Optimization of temporal sampling for <sup>82</sup>rubidium PET myocardial blood flow quantification. *J Nucl Cardiol* 2017. <https://doi.org/10.1007/s12350-017-0899-7>.
18. Ficaro E, Lee B, Kritzman J, Corbett J. Corridor4DM: The Michigan method for quantitative nuclear cardiology. *J Nucl Cardiol* 2007;14:455–65. <https://doi.org/10.1016/j.nuclcard.2007.06.006>.
19. Lortie M, Beanlands RSB, Yoshinaga K, Klein R, Dasilva JN, DeKemp RA. Quantification of myocardial blood flow with <sup>82</sup>Rb dynamic PET imaging. *Eur J Nucl Med Mol Imaging* 2007;34:1765–74.
20. Friedman J, Van Train K, Maddahi J, Rozanski A, Prigent F, Bietendorf J, et al. “Upward creep” of the heart: A frequent source of false-positive reversible defects during thallium-201 stress-redistribution SPECT. *J Nucl Med* 1989;30:1718–22.
21. Murthy VL, Bateman TM, Beanlands RS, Berman DS, Borges-Neto S, Chareonthaitawee P, et al. Clinical quantification of myocardial blood flow using PET: joint position paper of the SNMMI cardiovascular council and the ASNC. *J Nucl Med* 2017. <https://doi.org/10.2967/jnumed.117.201368>.